Available online at www.sciencedirect.com

SCIENCE DIRECT®

Engineering Geology 76 (2004) 109–128

ENGINEERING GEOLOGY

www.elsevier.com/locate/enggeo

Landslide hazard spatial analysis and prediction using GIS in the Xiaojiang watershed, Yunnan, China

H.X. Lan[a,*], C.H. Zhou[a], L.J. Wang[b], H.Y. Zhang[c], R.H. Li[c]

[a] *State Key Laboratory of Resources & Environmental Information System (LREIS), Institute of Geographical Sciences and Natural Resources Research, Chinese Academy of Sciences, Beijing 100101, PR China*

[b] *Institute of Remote Sensing Application, CAS, Beijing 100101, PR China*

[c] *Dezhou Seismological Bureau, Dezhou 253000, PR China*

Received 17 September 2002; accepted 7 June 2004
Available online 24 August 2004

Abstract

The Xiaojiang watershed in Southwest China has high landslide hazard and has been given the title of "the Museum of Geohazards in China". However, the available information on landslides in the Xiaojiang watershed is still limited. We constructed the essential spatial database of landslides using the GIS techniques. The quantitative relationships between landslides and factors affecting landslides are established by the Certainty Factor model (CF). The affecting factors such as lithology, structure, slope angle, slope aspect, elevation and off-fault distance are recognized. By applying CF value integration and landslide zonation, the most significant affecting factors are selected. The widespread landslide activities in the Xiaojiang watershed are caused and triggered by heavy rain. A promising approach to modeling the spatial distribution of rainfall-triggered landslide is combining the mechanistic infinite slope stability model with a hydrological model. A model modified from Stability INdex Mapping (SINMAP) is used to prepare the landslide susceptibility maps for different rainfall conditions. Information on these maps could be useful for explaining the known existing landslide, making emergency decisions and relieving the efforts on the avoidance and mitigation of future landslide hazards.

Keywords: The Xiaojang watershed (China); Landslide; Landslide hazard; Spatial analysis; GIS

1. Introduction

Landslides and debris flows rank high on the list of geohazards in the Xiaojiang watershed, Yunnan Province, Southwest China (Fig. 1). They are so serious that the Xiaojiang watershed comes to be known as "the Museum of Geohazards in China". Until the present, many publications have mainly dealt with the debris flows in the Xiaojiang watershed (Du et al., 1987; Wu et al., 1990). It should be noted that most of debris flows originally occur in the form of landslides before they move to valley channels. Landslide hazard poses a severe threat to life, property and infrastructure, and becomes a major constraint on the development of the Xiaojiang watershed. Strategies should be made to

* Corresponding author. Tel.: +86-10-64889764; fax: +86-10-64889630.
E-mail addresses: lanhx@lreis.ac.cn, lanhengxing@hotmail.com (H.X. Lan).

0013-7952/$ - see front matter © 2004 Elsevier B.V. All rights reserved.
doi:10.1016/j.enggeo.2004.06.009

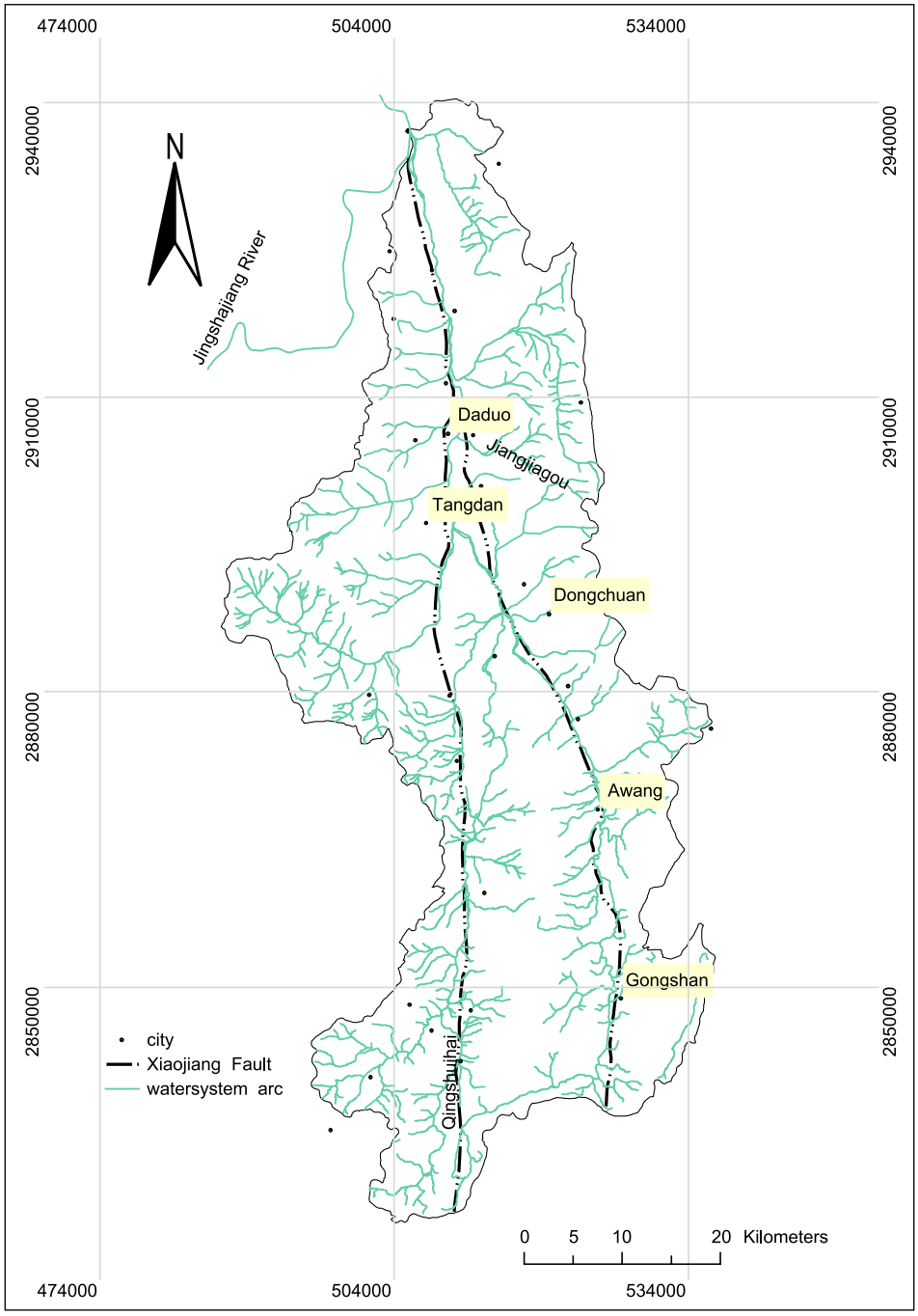

Fig. 1. Location of the study area. The Xiaojiang watershed is located in the Northeast part of Yunnan Province, China. The Xiaojiang deep fault passes through the whole watershed.

understand landslide process, analyze threatening landslide hazard and predict the future landslides for reducing ongoing and future damage from landslides.

GIS technologies could provide a powerful tool to model the landslide hazards for their spatial analysis and prediction. This is because the collection, manipulation and analysis of the environmental data on landslide hazard can be accomplished much more efficiently and cost effectively (Carrara and Guzzetti, 1999; Guzzetti et al., 1999). Many GIS-based analysis models and quantitative prediction models of landslide hazard have been proposed since the beginning of GIS application in geohazards research in the late 1980s (Carrara, 1983; Van Westen, 1994; Carrara et al., 1991, 1995, 1999; Jade and Sarkar, 1993; Chung et al., 1995, Chung and Fabbri, 1998, 1999, 2001).

Although landslides are among the major geohazards in the Xiaojiang watershed, the information on them is limited. The first essential step in this study is to establish spatial databases for landslides in ArcGIS (GIS software developed by ESRI), including landslides inventory data and the effecting factors (Armstron and Denaham, 1990; Kim et al., 1993). In order to relate landslide occurrences to the affecting factors, the Certainty Factor model (CF) is used in this research. The widespread landslide activities are mainly caused and triggered by heavy storm in the Xiaojiang watershed. A promising approach to model the spatial distribution of rainfall-triggered landslide combines a mechanistic infinite slope stability model with hydrological models (Grayson et al., 1992; Dietrich et al., 1995; Wu and Sidle, 1995; Pack et al., 1998). A model modified from Stability INdex Mapping (SINMAP) developed by Pack et al. (1998) is used to prepare the landslide susceptibility maps under different rainfall conditions. These maps could help to explain the known landslides, making emergency decisions, avoiding and mitigating of future landslide hazards. The landslide sensitive environment in the Xiaojiang watershed is defined by establishing the quantitative relationship between landslides and effecting factors using CF model and hazard zonation.

2. Spatial database

Data preparation is a first fundamental and essential step for landslide hazard analysis. The spatial database is mainly composed of two parts: landslide inventory and landslide affecting factors.

2.1. Landslide inventory

Creating the landslide inventory is fundamental for landslide hazard analysis based on GIS. Fig. 2 shows the landslide inventory map in the Xiaojiang watershed. Its compilation follows several procedures: (1) stereoscopic interpretation of multi-temporal vertical aerial photographs; (2) recognition of topographic features indicative of landslide landforms on aerial photographs and topographic maps, which can be finished by its combining with landslide data from previous investigations and information; (3) field verification of landside data and engineering geological classification of landslides; and (4) compilation of the landslide inventory map and digitization of data into ArcGIS.

The obtained landslide inventory of this area contains about six hundred landslides (Table 1). The landslides are subdivided into old landslides (326), new landslides (154), and landslips or scarps (94). They cover 87.353 km^2 or 3% of the entire study area. The new landslides and the landslips or scarps can be regrouped as active landslides, 43% of the total number of landslides. At this map, all landslides are represented by small polygons with different colors indicating different landslide groups.

2.2. Affecting factors

Some GIS-based landslide analysis models, such as statistical models, are based on the assumption that an area where landslides occur is now under prone-to-landslide environments, and that areas under those environments have high potential of new landslides occurrence, or future landslides will occur under circumstances similar to those of past landslides. Such prone environments are depicted by factors affecting the occurrence of landslides, such as rock and soil types, slope angles and landuse that are usually digitized as layers or themes in GIS.

In this study, seven categories of landslide affecting factors are selected and defined. They are lithologic group, rock mass structure group, distance to major faults, slope angle, slope aspect, and elevation. Each category is subdivided into different classes by its value or feature.

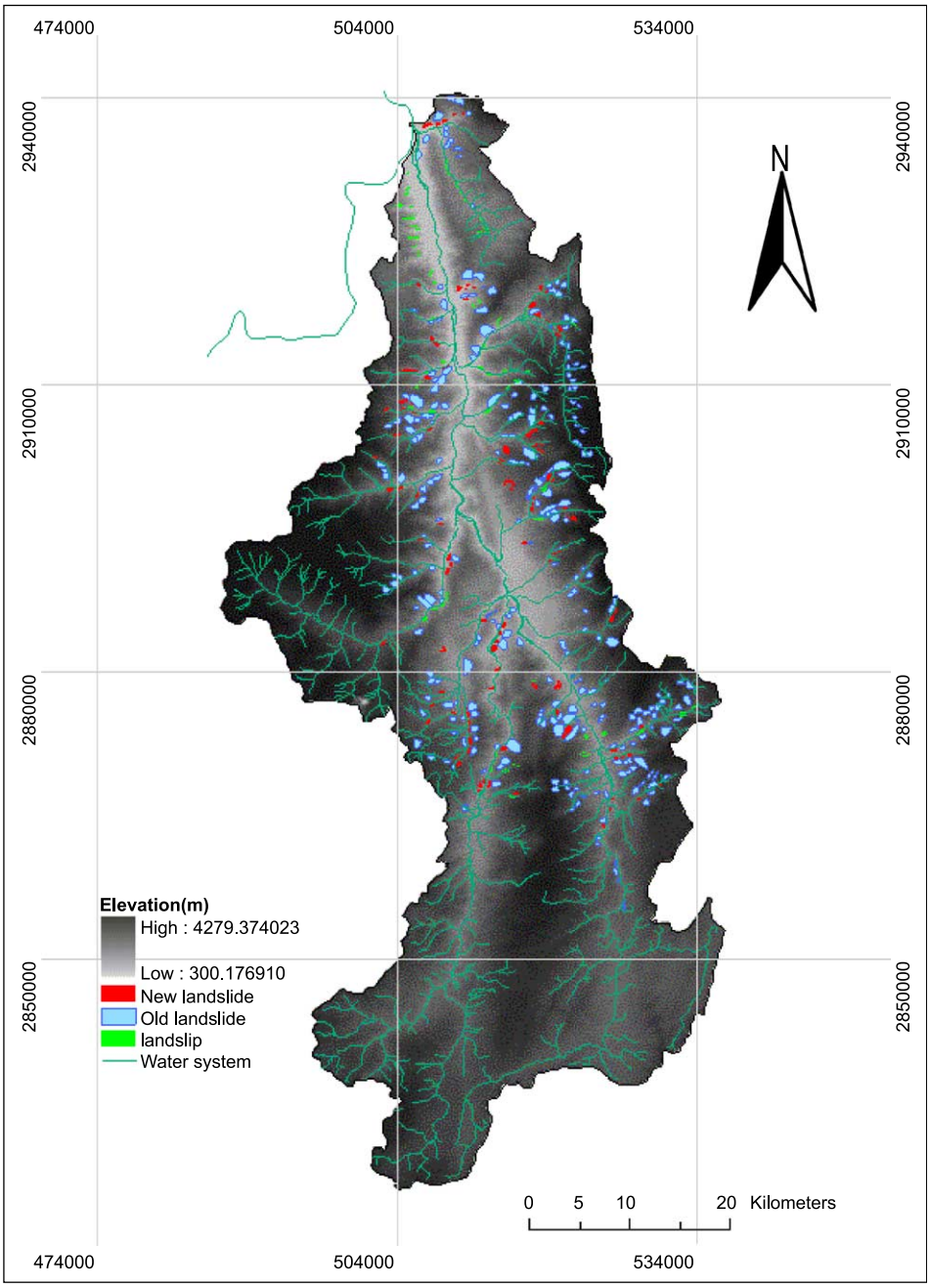

Fig. 2. Landslide inventory in the Xiaojiang watershed. The distribution of landslides is illustrated the DEM map of the Xiaojiang watershed. Different types of landslides are indicated by polygons with different gray levels.

2.2.1. Lithology

It is expected that lithology would be a major controlling factor for landsliding. A new simplified lithology map was prepared and digitalized, which was modified from the original geological map (Fig. 3). The strata on the map are classified into 16 lithologic

Table 1
Statistics of landslide types in Xiaojiang watershed

Landslide type		Number	Area (km^2)	Percent of watershed area (%)
No landslide or unknown zone		0	2955.647	97
Old landslide		326	87.123	2.9
Active landslide	New landslide	154	0.15	
	Landslip and scarps	94	0.08	0.0076

groups. These lithologic groups are composed of rocks with similar lithologic properties and geological ages (Table 2).

2.2.2. Rock mass structure

Rock mass structures have close relations to the mechanical characteristics of slopes. Physical and mechanical tests were performed on many representative samples from each lithology formation in the Xiaojiang watershed by Yunnan Diandong Engineering Exploration Corporation in 1993. These test data include rock mass strength, cohesion, internal friction, the spacing of discontinuity (structural plane), the state conditions of structural plane, and some other physical features (unit weight, moisture content, void ratio, etc.). They were then inputted in the spatial database in ArcGIS. The region lack of test data was evaluated by the test value mean of the corresponding samples in the similar geological formations. These data are classified into several groups by a certain rule. For example, the cohesion value was classified into five groups by equal interval and the internal friction angle was classified by natural breaks. These test data are useful for the classification of rock mass structure.

The classification of rock mass structure groups followed two major steps. First, rock mass structure was classified in terms of the spacing and feature of structure planes. For example, the rock masses with more than 50 cm of structure planes spacing were classified into massive structure group. The features of structure planes were then used for the sub-classification of rock mass. Second, each structural type was re-grouped into several groups according to rock strength test data, particularly the uniaxial compressive strength. For example, the rock masses with more than 30 Mpa of uniaxial compressive strength were classified into hard rock group. Finally, seven structure groups are obtained in the Xiaojiang watershed: hard rock massive structure (I_1), hard rock stratified structure (II_1), semi-hard rock stratified structure (II_2), hard rock interbeded with soft rock stratified structure (II_3), interlocked cataclastic structure (III_1), stratified cataclastic structure (III_2), and cataclastic structure (III_3). Their spatial distribution in the Xiaojiang watershed is shown in Fig. 4. Taking cataclastic structure (III_3) as an example, it is widely distributed in the downstream and middlestream of the Xiaojiang river. Its general engineering geological properties are: the average uniaxial compressive strength is 109.64 MPa; the average shear strength is 3.5 MPa; the average internal friction angle is 37°18′; and the average elastic modulus is 24.32×10^3 MPa.

2.2.3. Distance to major faults

The most significant fault in the Xiaojiang watershed is the Xiaojiang deep active fault. It passes through the whole watershed from the south to the north. Geometrically, it is composed of four fault sections: Xiaojing River outlet to Daduo, Daduo to Xiaoqinghai, Daduo to Awang, Awang to Gongshan. The distances of all pixels to each fault section are calculated and classified into three big categories for the convenience of interpreting (Table 3).

2.2.4. Slope angle, slope aspect and elevation

The slope angle, slope aspect and elevation data are extracted from the Digital Elevation Model (DEM) of the Xiaojiang watershed. This task has been implemented in ArcGIS by means of spatial extension model. The values of slope angle are divided into eight classes: 0–10°, 10–20°, 20–30°, 30–40°, 40–50°, 50–60°, 60–70° and more than 70°. The values of slope aspect are divided into eight classes with the 45° intervals. The values of elevation are divided into nine classes: 300–500, 500–1000, 1000–1500, 1500–2000, 2000–2500, 2500–3000, 3000–3500, 3500–4000 and more than 4000 m.

3. Landslide susceptibility

3.1. CF model

Among the commonly used GIS analysis models for landslide hazard, CF certainty model has been

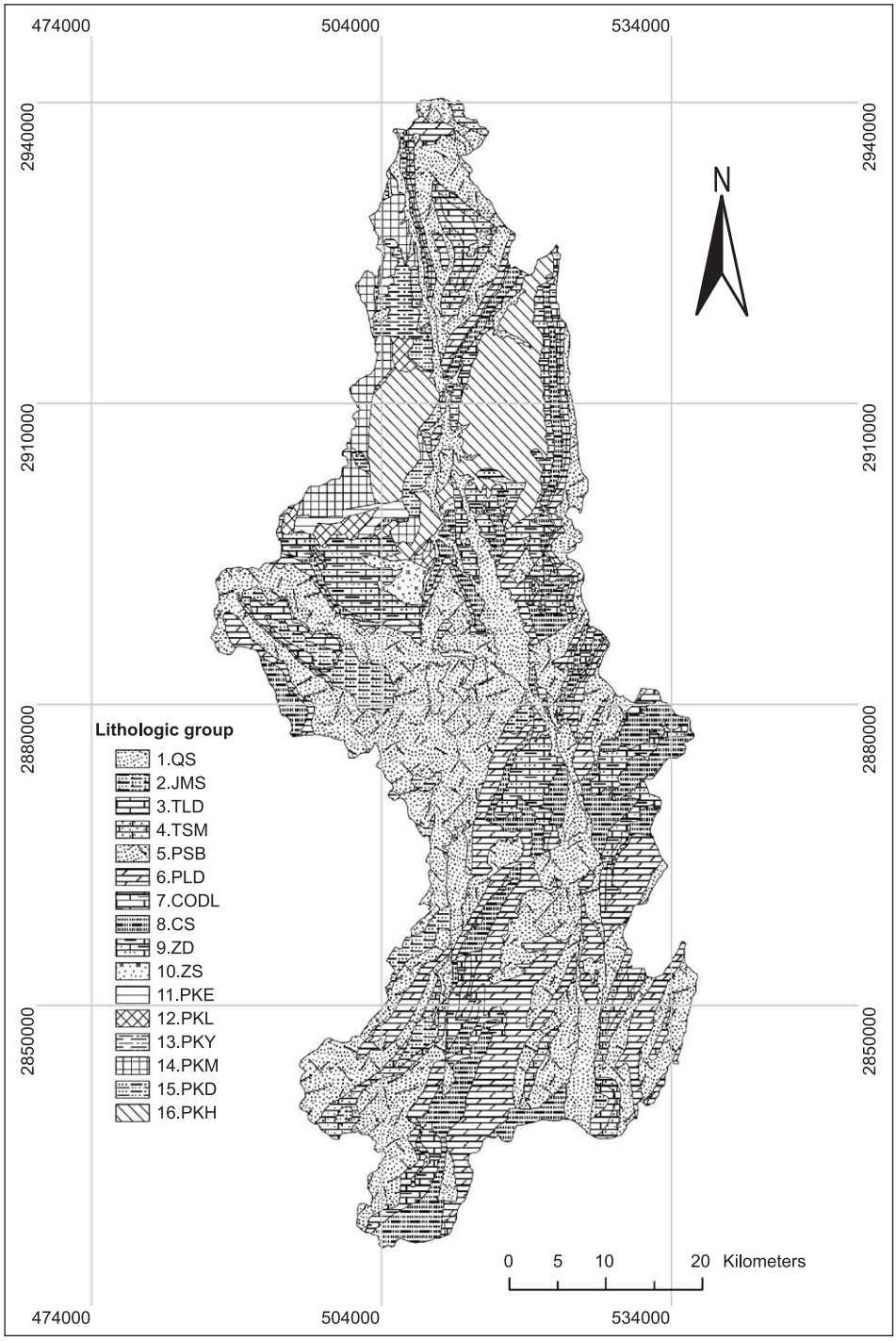

Fig. 3. Lithologic groups distribution. The study area can be divided into 16 lithologic groups, whose detail information is shown in Table 2.

Table 2
Lithologic groups classification

Code	Lithologic group
QS	Quaternary Sandstone
JMS	Jurassic Mudstone and Sandstone
TLD	Triassic Limestone and Dolomite
TSM	Triassic Sandstone and Mudstone
PSB	Permain Sandstone, Basalt
PLD	Permain Limestone and Dolomite
CODL	Carboniferous to Ordovician Dolomite, Limestone
CS	Cambrian Sandstone
ZD	Sinian Dolomite
ZS	Sinian Sand
PKE	Slate of Ertou Formation, Proterozonic Kunyang Group
PKL	Dolomite of Luoxue Formation, Proterozonic Kunyang Group
PKY	Slate clip dolomite of Yinmin Formation, Proterozonic Kunyang Group
PKM	Slate of Miedang Formation, Proterozonic Kunyang Group
PKD	Dolomite and limestone of Dalong Formation, Proterozonic Kunyang Group
PKH	Slate and dolomite of Heitoushan–Caoling Formation, Proterozonic Kunyang Group

deeply considered and experimentally investigated (Chung and Fabbri, 1993, 1998; Binaghi et al., 1998; Luzi and Pergalani, 1999). The Certainty Factor (CF) approach is one of the possible proposed Favourability Functions (FF) to handle the problem of combination of different data layers and the heterogeneity and uncertainty of the input data. The CF, defined as a function of probability, was originally proposed by Shortliffe and Buchanan (1975) and later modified by Heckerman (1986):

$$\mathrm{CF} = \begin{cases} \frac{pp_a - pp_s}{pp_a(1-pp_s)} & \text{if } pp_a \geq pp_s \\ \frac{pp_a - pp_s}{pp_s(1-pp_a)} & \text{if } pp_a < pp_s \end{cases} \quad (1)$$

where pp_a is the conditional probability of having a number of landslide event occurring in class a and pp_s is the prior probability of having the total number of landslide events occurring in the study area A.

The range of variation of the CF is [−1.1]: positive value means an increasing certainty in landslide occurrence, while negative value corresponds to a decreasing certainty in landslide occurrence. A value close to 0 means that the prior probability is very similar to the conditional one, so it is difficult to give any indication about the certainty of the landslide occurrence.

The favourability values (pp_a, pp_s) are derived from overlaying each data layer with the landslide inventory layer in ArcGIS and calculating the landslide occurrence frequency. And CF values are then calculated for each layer (lothologic group, rock mass structure group, slope angle, etc.) in the Xiaojiang watershed. For example, in order to calculate the landslide Certainty Factor (CF) of the terrain with slope in the range from 30° to 40°, we first classified the slope layer by 10° interval as mentioned above. Then, the landslide inventory layer overlaid the classified slope layer in ArcGIS, and we got a new layer that contains the information of both slope gradient and landside occurrence. For slope class 30–40°, we first calculated the area of landslide falling in this class and divided it by the total area of this class, and this way we obtained the favourability value pp_a. Likely, the value pp_s was calculated by dividing the total area of landslide with the total area of the watershed. Inputting the pp_a and pp_s into expression (1), the CF value of slope class 30–40° was finally calculated. After calculating the CF value of each class for all layers, the layers were then combined pairwise according to the integration rules (Chung and Fabbri, 1993). Binaghi et al. (1998) also described the detailed steps of CF calculating and integrating.

3.2. Lithologic group and landslide

It is expected that lithology would be a major controlling factor for landsliding, since landslides are concentrated on certain lithologic units. The distribution of lithology reflects the much different topography developed on those lighologic groups as well as the structure, strength and stress distribution of slope. From the result of lithologic groups certainty factor (CF) (Table 4), it can be seen that the suitable lithologic groups for landslide occurrence and development are Proterozonic Kunyang Group (PK), Sinian formation (ZD and ZS), Cambrian formation (CS) and Quaternary deposite (QS). The highest landslide certainty is found on unit PKE (slate of the Ertou Formation, Proterozonic Kunyang Group), PKD (dolomite and limestone of the Dalong Formation), PKH (slate and dolomite of the Heitoushan–Caoling Formation), ZD (Sinian

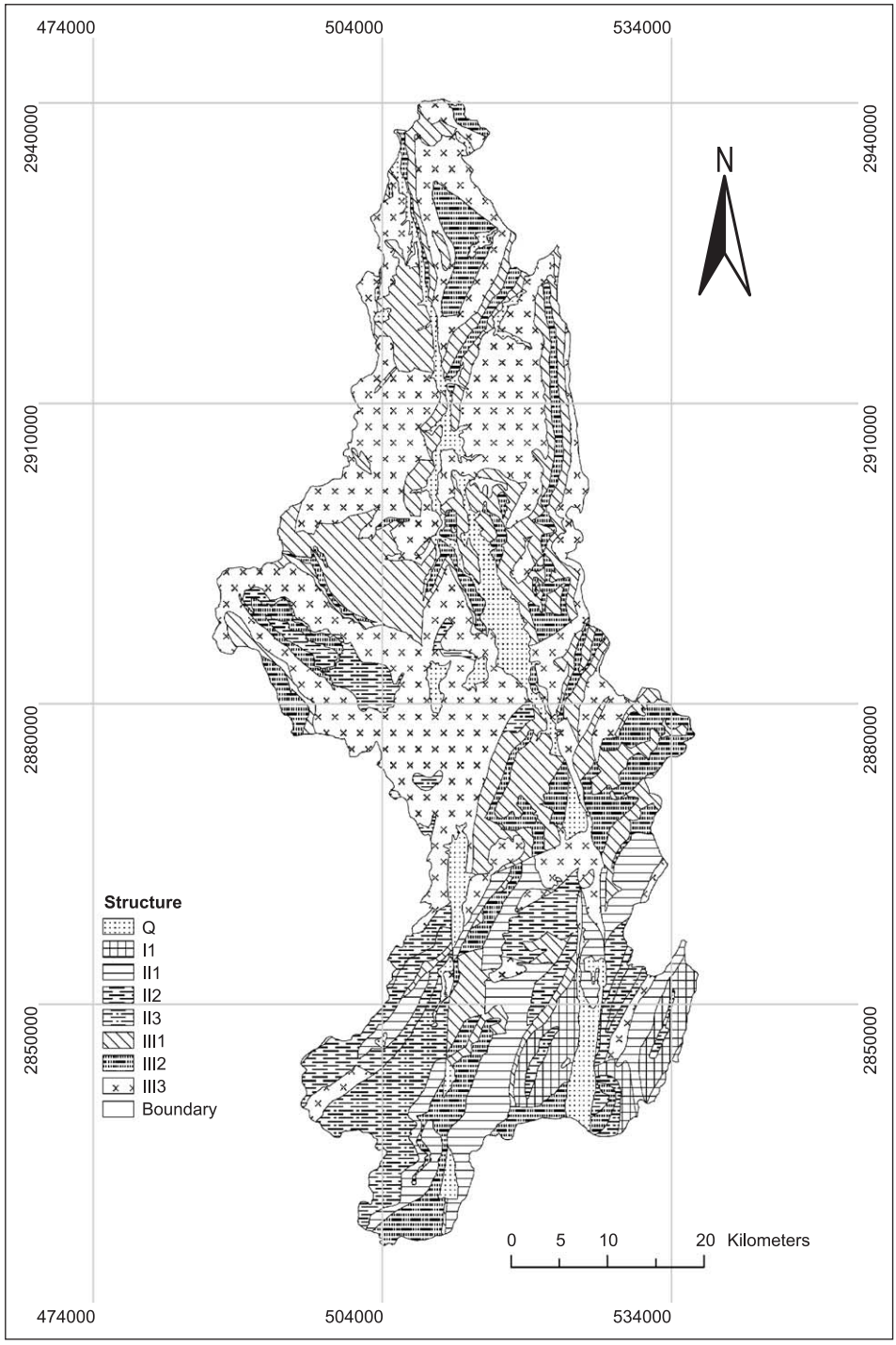

Fig. 4. Rock mass structure groups distribution in the Xiaojiang watershed. Seven structural classes are recognized according to the physical and mechanical properties of rock masses as well as the feature of structure planes.

Table 3
Distance to Xiaojiang fault

Code	Fault section	Distance (m)
11	Xiaojiang River outlet to Daduo	500
12	Xiaojiang River outlet to Daduo	2000
13	Xiaojiang River outlet to Daduo	4000
21	Daduo–Qingshuihai	500
22	Daduo–Qingshuihai	2000
23	Daduo–Qingshuihai	4000
31	Daduo–Awang	500
32	Daduo–Awang	2000
33	Daduo–Awang	4000
41	Awang–Gongshan	500
42	Awang–Gongshan	2000
43	Awang–Gongshan	4000
0	Whole Xiaojiang Fault	>4000

dolomite), CS (Cambrian sand) and QS (Quaternary sand), whose CF value are near or more than 0.5, indicating a high landslide susceptibility.

3.3. Structure group and landslide

Rock mass structure groups with CF more than zero unexpectedly fall in class III (interlocked cataclastic structure (III_1), stratified cataclastic structure (III_2), cataclastic structure (III_3)), in which rock masses are severe fractured and altered, and unit with interlocked structure is the most susceptible for landsliding in the Xiaojiang watershed (Table 5). The significant landslide controlling effect of rock mass structure is dependent on weak structure planes that could easily convert to landslide planes and strongly effect the mechanical features of landslide masses.

Table 4
CF value of lithologic group

Code	Area of lithologic group (km^2)	Area of landslides in each class (km^2)	Landslide frequency (%)	CF
QS	173.137	9.729	5.619	0.279
JMS	94.111	0.935	0.993	−0.766
TLD	88.851	2.817	3.171	−0.237
TSM	48.396	1.186	2.450	−0.415
PSB	949.676	28.737	3.026	−0.273
PLD	408.498	15.839	3.877	−0.061
CODL	90.012	5.827	6.474	0.379
CS	299.271	26.086	8.717	0.550
ZD	225.093	36.295	16.124	0.777
ZS	18.250	0.829	4.545	0.098
PKE	21.708	1.609	7.412	0.464
PKL	25.582	0.892	3.485	−0.159
PKY	29.720	1.346	4.530	0.009
PKM	125.657	4.839	3.851	−0.067
PKD	26.623	3.747	14.075	0.608
PKH	224.429	30.836	13.741	0.730

Table 5
CF value of structure group

Code	Area of structure group (km^2)	Area of landside in each group (km^2)	Landslide frequency (%)	CF
I1	91.075	0.000	0.000	−1.000
II_1	240.692	0.208	0.087	−0.978
II_2	132.895	0.268	0.202	−0.953
II_3	217.058	0.749	0.345	−0.919
III_1	583.086	39.768	6.820	0.410
III_2	372.154	17.868	4.801	0.173
III_3	1038.917	52.002	5.005	0.185
Q	173.137	3.765080	2.175	0.279

3.4. Distance to major fault and landslide

Generally, rock masses near the Xiaojiang deep fault zone are less intact and severe fractured. According to investigation, the Xiaojiang deep fault is a dominant factor controlling the development of all types of landslides. Table 6 shows the CF value of each fault zone. It may be confused that the landslide certainty of classes far from the fault

Table 6
CF value of distance to Xiaojiang fault

Code	Distance to fault (m)	Area of each class (km^2)	Area of landsides in each class (km^2)	Landslide frequency (%)	CF
11	500	26.794	0.923	3.446	−0.169
12	2000	77.906	5.539	7.110	0.439
13	4000	97.273	8.953	9.204	0.576
21	500	82.886	2.407	2.905	−0.302
22	2000	237.175	12.003	5.061	0.194
23	4000	267.063	10.544	3.948	−0.043
31	500	44.043	0.517	1.173	−0.590
32	2000	121.726	8.499	6.982	0.427
33	4000	136.644	13.059	9.557	0.594
41	500	31.987	1.212	3.788	−0.010
42	2000	94.920	0.763	0.803	−0.980
43	4000	116.835	1.814	1.553	−0.632
0	>4000	1450.175	48.395	3.337	−0.196

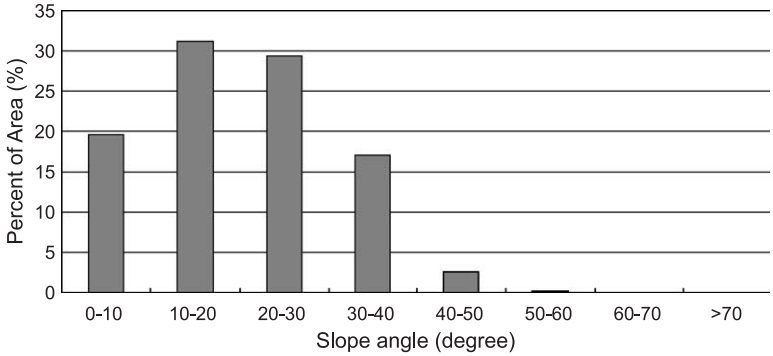

Fig. 5. Statistical map of slope angle distribution in the Xiaojiang watershed.

zone has high CF value. It is probably because that the defined class span of a large range of landslides is not a preferred technique and each factor always controls landslide occurrence is along with other factors (such as slope, aspect, and lithology). Nevertheless, we can see from the CF value of each class that the different fault section has different controlling effect on landslides. In the Xiaojiang watershed, it decreases in the following sequence: the section from outlet to Daduo, the section from Daduo to Awang, the section from Daduo to Qingshuihai, the section from Awang to Gongshan.

3.5. Geomorphology and landslide

3.5.1. Slope angle

The slopes in the Xiaojiang watershed are characterized by low and medium high angles. The slopes with angles lower than 40° cover most of the study area (Fig. 5). There are lack of slopes steeper than 50°. The highest CF values are found in two classes of slopes: one with the slope angle ranging from 30° to 40° and one with the slope angle ranging from 40° to 50° (Fig. 6). The CF value of slopes with the slope angles lower than 20° is negative, which means a low probability of landslide occurrence. In general, the landslide frequency increases with increasing of the slope angle in the range of 0–50°. Slopes steeper than 60° are rare. So its CF value is about −1.

3.5.2. Slope aspect

The landslide frequency is also controlled by the slope aspect. In the Xiaojiang watershed, the slopes classes unexposed to sun such as slopes facing NW (CF 0.339) and the slopes facing N (CF 0.166) have high CF values indicative of increasing landsliding (Table 7). The shaded slopes have lower ground temperature, higher soil moisture, thicker residuum and colluvium mantles, thicker vegetation, and less

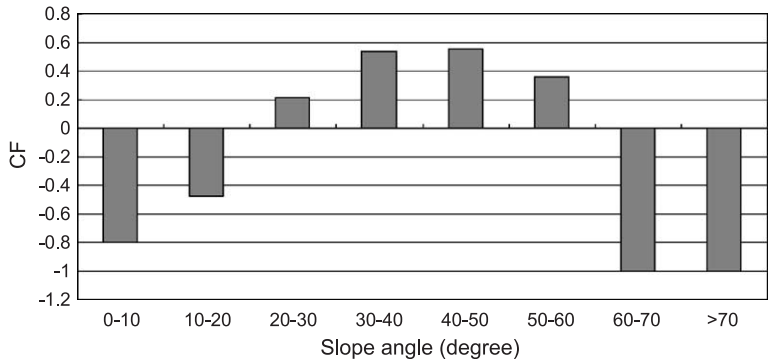

Fig. 6. CF value of slope angle layer. The class with high CF value has high landslide hazard.

Table 7
CF value of slope aspect layer

Slope aspect	Area of aspect class (km^2)	Area of landslides in each class (km^2)	Landslide frequency (%)	CF
N	278.710	13,679,478.335	4.900	0.166
NE	323.008	11,400,248.944	3.500	−0.155
E	381.511	11,022,466.863	2.900	−0.300
SE	388.605	13,907,244.081	3.600	−0.130
S	291.904	16,479,417.796	5.600	0.276
SW	314.919	10,152,650.169	3.200	−0.230
W	429.496	14,640,267.213	3.400	−0.180
NW	377.030	23,174,486.234	6.100	0.339

sheet wash and erosion, which are favorable for landslide occurrence. As for slopes facing the sun with high CF value, such as the class S with CF value 0.276, they could be interpreted by the strong river incision. This phenomenon is very common in many sub-watersheds, such as the slopes in the Jiangjiagou sub-watershed.

3.5.3. Elevation

The landslides are mostly distributed in areas belonging to lower and middle elevation classes. The slopes falling in elevation classes of 500–2000 m have the highest CF value (Fig. 7). Like the slope aspect, elevation is not the direct affecting factor on landslide event, but it can control several other factors, especially vegetation, river wash and incision, and soil erosion.

Table 8
Hazard classification by CF value

Code	Range	Description	Hazard class
1	−1, −0.5	Very low certainty of landslide occurrence	High stability
2	−0.5, −0.05	Low certainty of landslide occurrence	Medium stability
3	−0.05, 0.05	Uncertainty. CF value within the range close to zero represent the interval in which no landsliding certainty can be expressed	Uncertainty
4	0.05, 0.3	Low certainty of landslide occurrence	Low instability
5	0.3, 0.8	Medium certainty of landslide occurrence	Medium instability
6	0.8, 1.0	High certainty of landslide occurrence	High instability

3.6. Determination of significant factors

Data layers were combined using the CF integration rule in ArcGIS. First two layers are combined to generate a new map, which then is combined with the third one, continuing until the last layer was integrated. The integrated CF values are classified into six hazard classes as shown in Table 8 to make the results easier to understand. The active landslide map (including new landslides and landslips) is overlaid with each combined layer of reclassified CF values (hazard

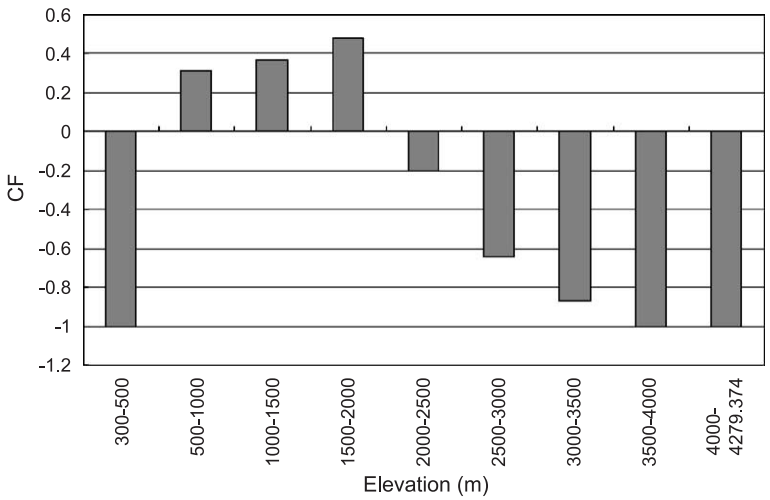

Fig. 7. CF value of elevation layer. The class with high CF value has high landslide hazard.

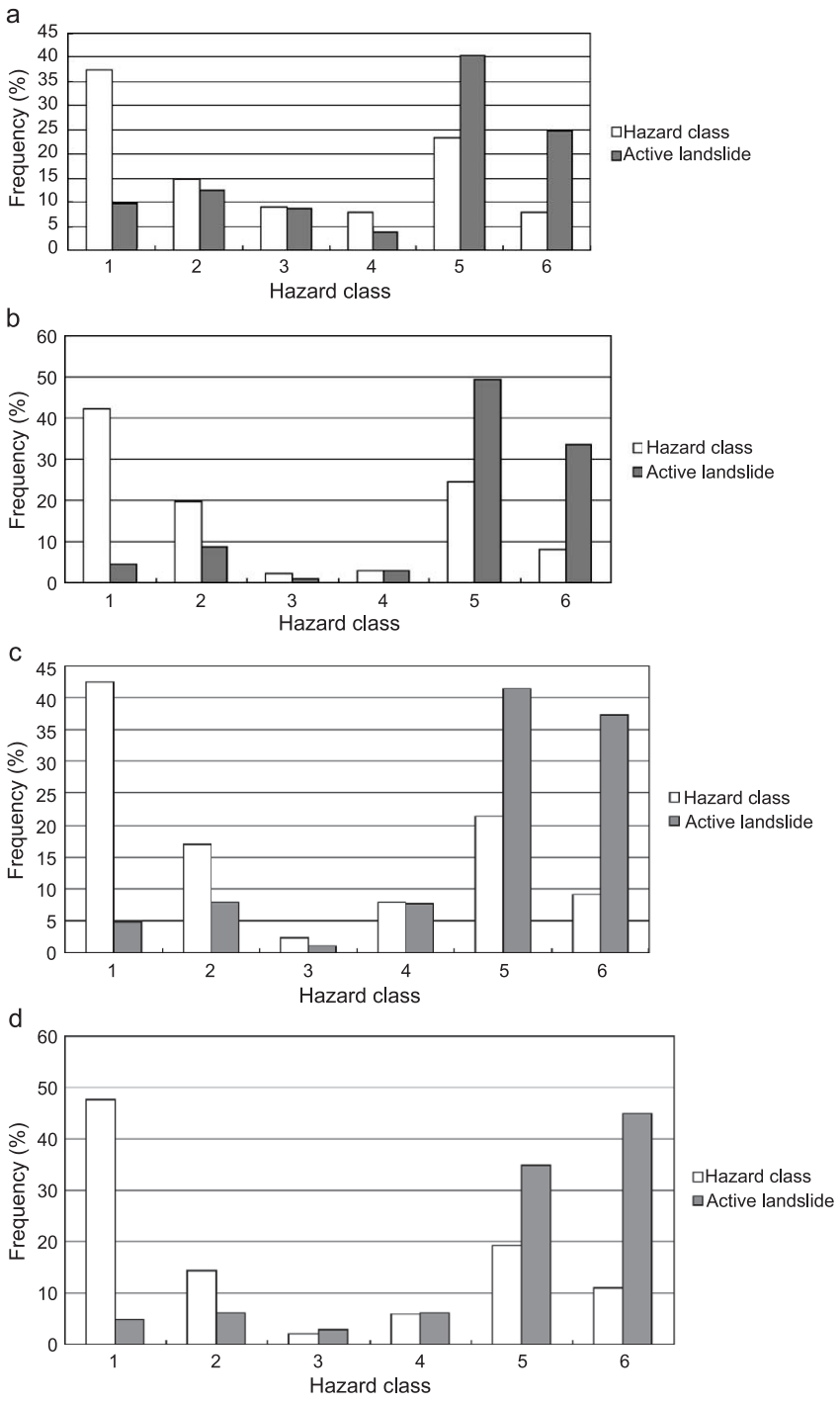

Fig. 8. (a) Results by overlaying three layers (lithologic groups, structure groups and slope angle). (b) Results by overlaying four layers (lithologic groups, structure groups, slope angle and elevation). (c) Results by overlaying five layers (lithologic groups, structure groups, slope angle, elevation and slope aspect). (d) Results by overlaying six layers (lithologic groups, structure groups, slope angle, elevation, slope aspect and off-fault distance layer).

Table 9
Landslide hazard class definitions by SI

SI	Class	Stability
SI>1.5	1	High stability
1.5>SI>1.25	2	Medium stability
1.25>SI>1.0	3	Low stability
1.0>SI>0.5	4	Low instability
0.5>SI>0.0	5	Medium instability
SI=0	6	High instability

class). Both the frequency of landslide within each hazard class, normalized to the total landslide area and the frequency of each hazard class, normalized to the total study area, are calculated.

In this study, the first combination is between ligholigical groups layer, structure groups layer and then slopes angle layer. The classes 5 and 6 indicating highest hazard explained 65% of the active landslide occurrence, while class 3 does 8.6% (Fig. 8a). The relatively high frequency of landslide in class 3 means that the more information are needed to assess the landslide hazard, or that there are errors during the field work or the data processing. When adding the more information of elevation, the result showed an increasing accuracy of landslide prediction (Fig. 8b). Classes 5 and 6 explain 83% of landslide, class 6 34%, and the class 3 only 1%. After combining the slope aspect layer, the landslides explained by class 3 almost remained constant, those explained by class 6 increased slightly, but those by classes 5 and 6 together decreased (Fig. 8c). This shows that slope aspect has slight relationship to landslide occurrence. When adding the layer of off-fault distance, the active landslides that the highest class 6 could explain increased by 8%, from 37% to 45% (Fig. 8d), indicating an increasing accuracy of hazard analysis. From above, it follows that lithology, structure, slope angle and distance to fault are the most significant factors for landsliding in the Xiaojiang watershed.

4. Spatial prediction

4.1. Prediction model

Most landslides in the Xiaojiang watershed are rainfall-triggered. The physical relationship between rainfall and landslide failure has long been investigated. There are two main approaches for rainfall-triggered landslide prediction: (1) use statistical correlations and forecasting techniques to establish the empirical relationships between rainfall and landslide; (2) use a deterministic model coupling a mechanistic slope stability model with a hydrological model to model groundwater recharge and pore water pressure changes caused by rainfall. Many researchers have been engaged in the slope failure or landslide hazard analysis with models similar to second approach (Dietrich et al., 1995; Montgomery and Dietrich, 1994; Wu and Sidle, 1995; Pack et al., 1998; Connell et al., 2001). However, most models are valuable for certain applications and certain region. For common application, the SINMAP (Stability Index MAPping) model constructed by Pack et al. (1998) integrated infinite slope stability model and the steady state hydrologic model based on TOPMODEL (Beven and Kirkby, 1979; Connell et al., 2001). Detail discussion of SINMAP model was presented in Pack et al. (1998). We made it a minor modification by adding the hydrodynamic pressure for simulating the groundwater seepage force. The basic model expression changed into:

$$\mathrm{Fs} = \frac{C' + (1 - \mathrm{Min}\left(\frac{q}{T}\frac{a}{\sin\theta}, 1\right)\frac{1}{r})\cos^2\theta\tan\phi}{(1 + \mathrm{Min}\left(\frac{q}{T}\frac{a}{\sin\theta}, 1\right)\frac{1}{r})\cos\theta\sin\theta} \quad (2)$$

where C_s' is $C/Z\gamma_s$, r is γ_s/γ_w, C is cohesion (kPa), γ_s is the density of landslide soil (kN/m^3), γ_w is the density of water (kN/m^3), Z is the depth of the vertical landslide body (m), θ is slope angle, ϕ is internal friction angle, q is effective rainfall with its value = real rainfall − evaporation − infiltration, is the transmissivity of landslide soil (m^2/h) and a is the specific catchment area.

Table 10
Relationship between real precipitation and T/q

Real precipitation (mm/day)	T/q (m)
20	5000
30	3300
40	2500
60	1700
80	1250
100	1000
120	830
140	730

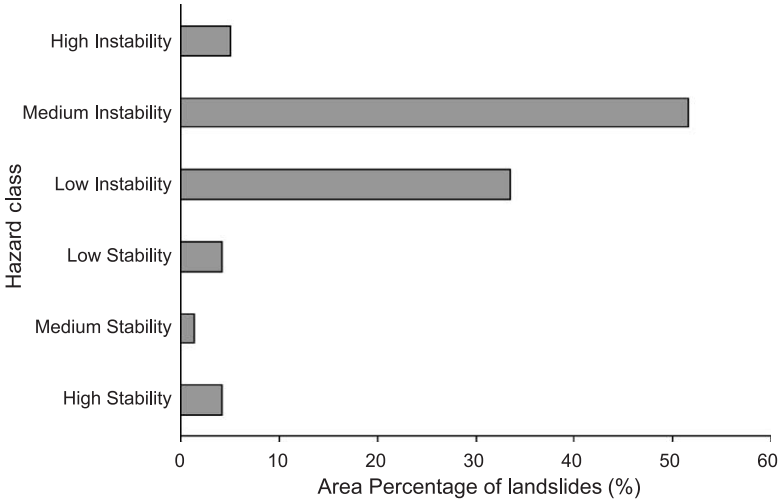

Fig. 9. Statistical analysis of modeling results. The percentages in the landslide area of each hazard class/the total landslide area are calculated.

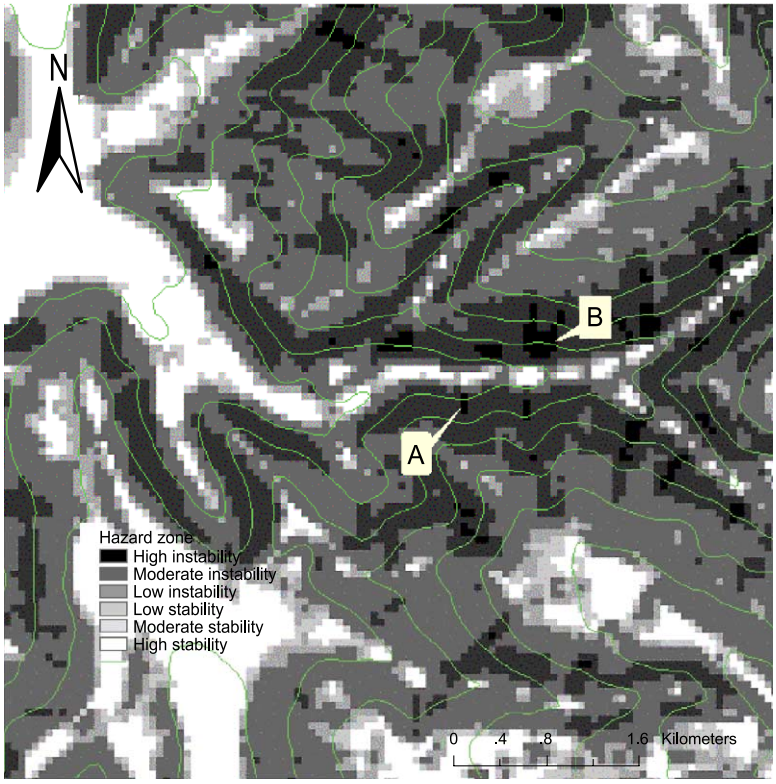

Fig. 10. Hazard modeling result in the Jiangjiagou sub-watershed. Area A and Area B are classified as high instable class.

Fig. 11. Photograph of a landslide in area A. The landslide occurred with age of less than half year before the field test in October, 2000.

The stability index (SI) is defined as the probability of the slope stability over the distributions of the uncertain parameters interval of C, ϕ, q, T. That is

$$\mathrm{SI} = \mathrm{Prob}(\mathrm{Fs} > 1) \tag{3}$$

The classes of landslide hazard classes are defined by SI, as shown in Table 9.

4.2. Input parameters

According to the model description mentioned above, we need to consider the variables a, θ, r, C, ϕ, T, q. The specific catchment area a and the slope angle θ are derived from DEM. The other variables can be obtained or calculated from engineering geotechnical

Fig. 12. Photograph of a landslide in area B, the right-bottom part of landslide is under sliding during the field verification in October, 2000.

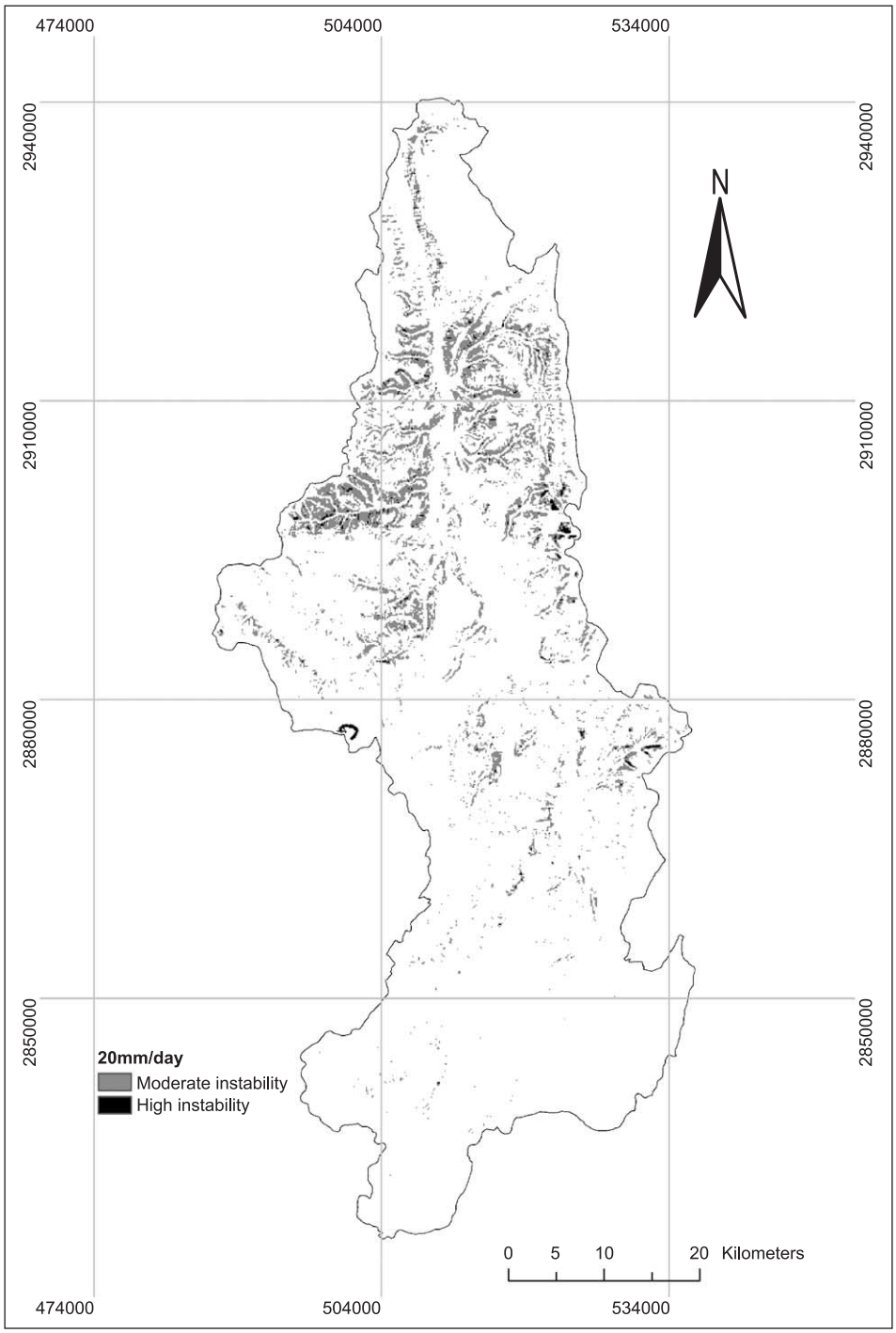

Fig. 13. (a) Spatial distribution of landslide hazards (high instability and moderate instability) under the precipitation value 20 mm/day. (b) Spatial distribution of landslide hazards (High instability and moderate instability) under precipitation value 120 mm/day. The area of instability increases significantly with the increase of precipitation values.

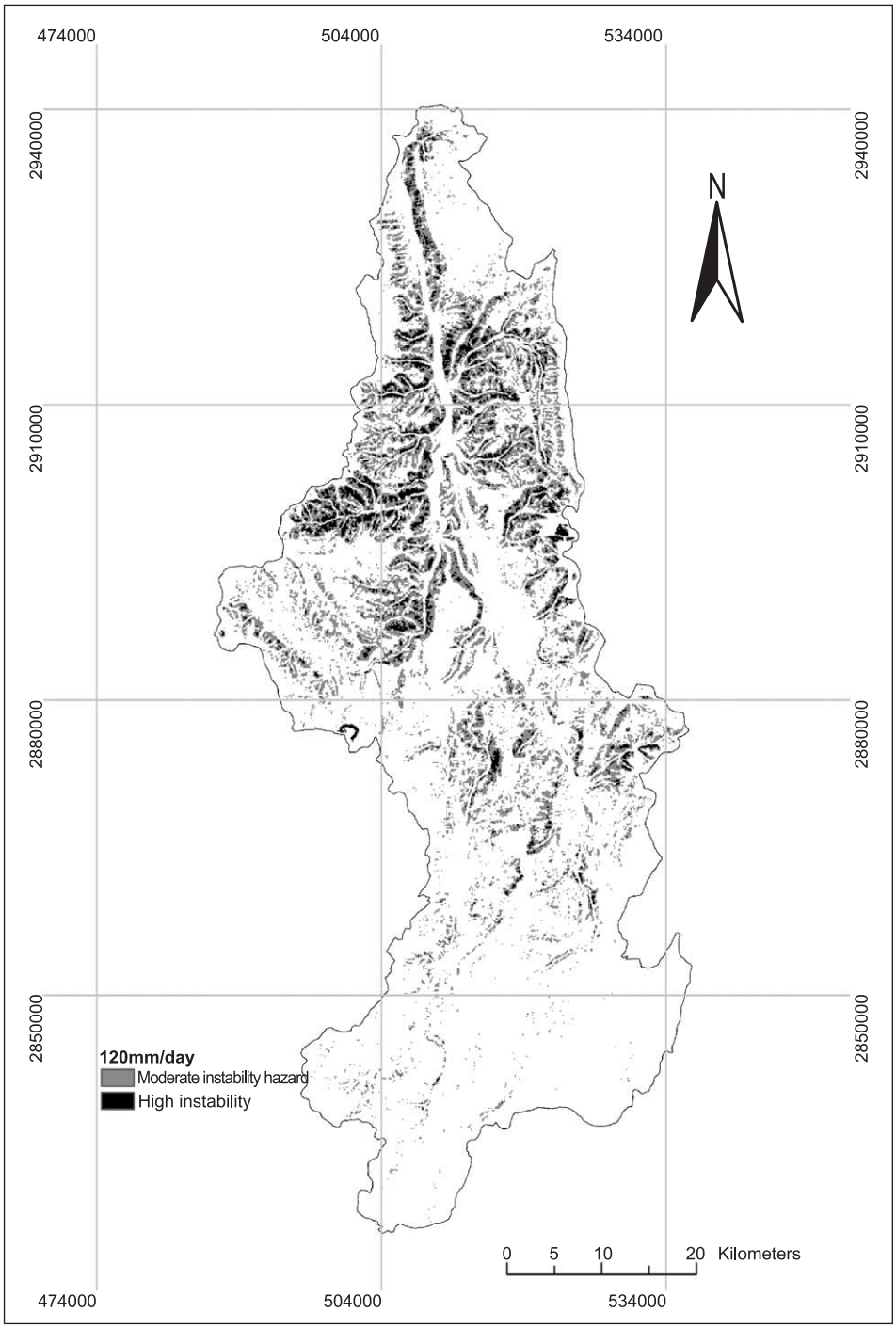

Fig. 13 (*continued*).

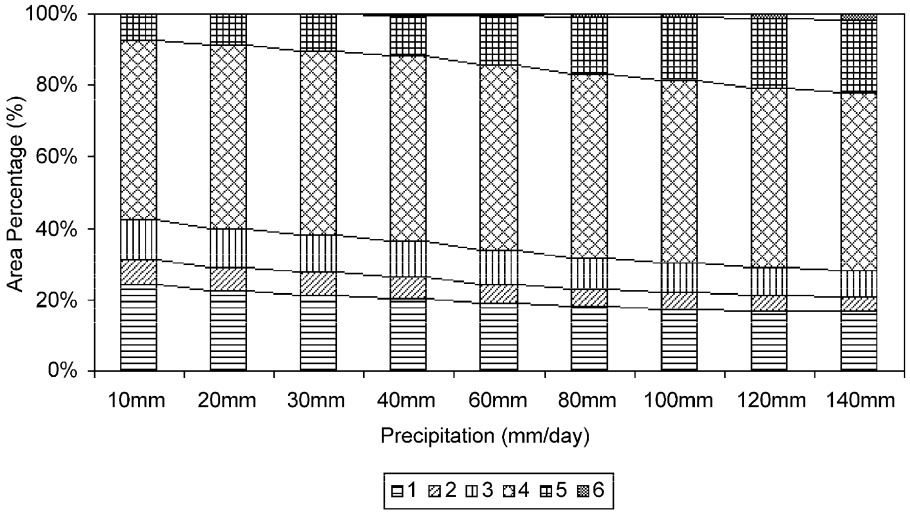

Fig. 14. The hazard area changes with precipitation. The percentage is the area of each hazard class/the total area of the watershed. (1) High Stability; (2) Medium Stability; (3) Low Stability; (4) Low Instability; (5) Medium Instability; (6) High Instability.

parameter database mentioned above. The effective rainfall q can be evaluated from real rainfall. Taking T/q as a single parameter, we have Table 10 to indicate the relationship between real precipitation and T/q.

4.3. Analytical results

The landslide stability maps for different precipitation conditions are drawn by the modified SINMAP model using DEM, landslide inventory data, and engineering geotechnical parameters. In order to check the suitability of the model in the Xiaojiang watershed, we prepared a landslide hazard map for the real average maximum precipitation of the Xiaojiang watershed and did statistical analysis. Statistical results show that the predicted instable classes can explain 90% of known landslides (Fig. 9). The landslides falling into stable classes are less than 10% of

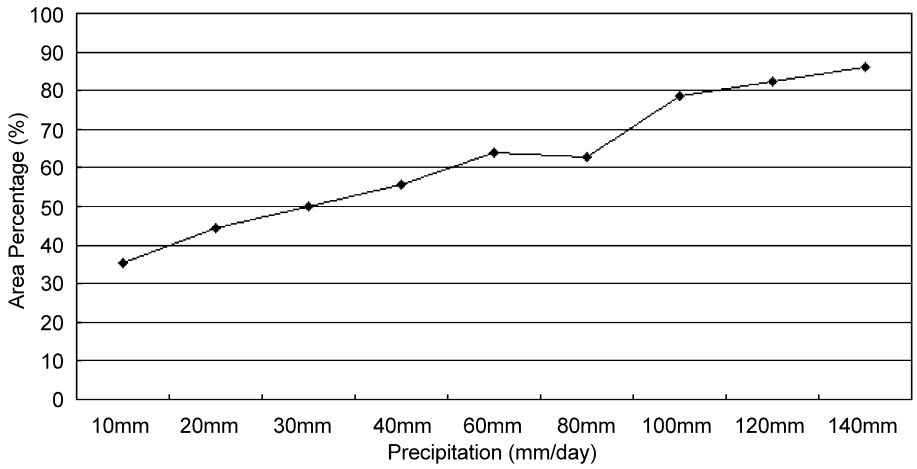

Fig. 15. Statistical analysis of active landslide areas in instable classes with the increase of precipitation value. The percentage is the area of landslides in instable classes (class 5 and 6)/the total landslide area.

total landslides. A detailed field investigation was carried out in the Jiangjiagou sub-watershed to test the validation of the predicted hazard map (Fig. 10). For example, in area A and area B belonging to the highest hazard class, new landslides with age less than half year were discovered (Figs. 11 and 12). The right bottom of a landslide in area B was under sliding during our field investigation in October, 2000.

A landslide hazard map for future precipitation conditions was constructed for the establishment of regional scale warning system. The comparison between the landslide hazard map under precipitations 20 mm/day (Fig. 13a) and 120 mm/day (Fig. 13b) present a visualizing way to understand the spatial distribution trend and pattern of landslide instability clearly. Landslides become increasingly abundant as the precipitation value increases. Most of them are concentrated on the downstream and middle stream area of the Xiaojiang River. The areas falling in instable classes increase dramatically with the increase of precipitation values, while the areas falling in stable classes decreases. As the precipitation value increases from 10 to 140 mm/day, the areas falling in of instable classes (high instability and medium instability) increase from 7.2% to 22.1% of the total area of the watershed (Fig. 14). The transiting area from the stable classes to the instable classes remains about constant 50% of the total watershed area. When the precipitation value increases up to 110 mm/day, 80% of the known landslides will become instable (high instability and medium instability) (Fig. 15). At this time, it is reasonable to predict that almost of the landslides will occur. Therefore the threshold precipitation value in the Xiaojiang watershed can be estimated as 110 mm/day.

5. Conclusions

Landslide events in the Xiaojiang watershed are strongly correlated to many factors. Factor susceptive analysis relies on landslide inventory data mainly obtained from field investigation and aerial photograph interpretation. The quantitative relationship between affecting factors and landslides can be achieved by the Certainty Factor method (CF). The indicators most sensitive to landslide in the Xiaojiang watershed are: (1) The Ertou Formation of the Proterozonic Kunyang Group, the Dalong Formation, the Heitoushan–Caoling Formation and Sinian dolomite and Cambrian sandstone; (2) Cataclastic structure, especially interlocked cataclastic structure; (3) Slope angles of 30–50; (4) Slope facing S, N and NW; (5) Elevation of 500–2000 m; (6) The outlet to Daduo section and Daduo to Awang section of the Xiaojang deep fault.

According to the results of CF value integration and landslide hazard zonation, key affecting factors are defined, which provide useful information for identifying different levels of landslide hazard.

Most landslides in the Xiaojiang watershed belong to the rainfall-triggered. The combination of a deterministic stability model with a hydrological model provides a powerful tool for predicting the rainfall-triggered landslides. The model modified from SINMAP cannot only assess and explain the areas where landsliding has already occurred, but also predict the potential hazard areas where landslide will occur under future precipitation conditions. The information provided by the hazard maps under different rainfall conditions could help citizens, planners and engineers to reduce losses caused by existing and future landslides by means of prevention, mitigation and avoidance.

Acknowledgements

This work was supported by the Chinese natural science fund (Grant No. 40225004) and special project of Chinese Academy of Science “Mountainous hazard—fundamental research on landslide and debris flow”. The authors would like to express their appreciation to Professors S.J. Wang and F.Q. Wu for detailed comments and suggestion. Additionally, the authors wish to thank the Institute of Mountain Hazard and Environment, CAS for kindly providing corresponding data.

References

Armstron, M.C., Denaham, P.J., 1990. Database organization strategies for spatial decision support systems. International Journal of Geographic Information System 4 (1), 3–20.

Beven, K.J., Kirkby, M.J., 1979. A physically based, variable contributing area model of basin hydrology. Hydrological Science Bulletin 24, 43–69.

Binaghi, E., Luzi, L., Madella, P., 1998. Slope instability zonation: a comparison between certainty factor and fuzzy Dempster–Shafer approaches. Natural Hazards 17, 77–97.

Carrara, A., 1983. Multivariate methods for landslide hazard evaluation. Mathematical Geology 15, 403–426.

Carrara, A., Guzzetti, F., 1999. Use of GIS technology in the prediction and monitoring of landslide hazard. Natural Hazards 20, 117–135.

Carrara, A., Cardinali, M., Detti, R., Guzzetti, F., Pasqui, V., Reichenbach, P., 1991. GIS techniques and statistical models in evaluating landslide hazard. Earth Surface Processes and Landforms 16, 427–445.

Carrara, A., Cardinali, M., Guzzetti, F., Reichenbach, P., 1995. GIS technology in mapping landslide hazard. In: Carrara, A., Guzzetti, F. (Eds.), Geographical Information Systems in Assessing Natural Hazards. Kluwer Academic Publishers, Dordrecht, The Netherlands, pp. 135–175.

Chung, C.F., Fabbri, A.G., 1993. Representation of geoscience data for information integration. Journal of Non-Renewable Resources 2 (2), 122–139.

Chung, C.F., Fabbri, A.G., 1998. Three Bayesian prediction models for landslide hazard. In: Buccianti, A. (Ed.), Proceedings of International Association for Mathematical Geology 1998 Annual Meeting (IAMG.98), Ischia, Italy, October 3–7, 1998, pp. 204–211.

Chung, C.F., Fabbri, A.G., 1999. Probabilistic prediction models for landslide hazard mapping. Photogrammetric Engineering and Remote Sensing (PE&RS) 65 (12), 1388–1399.

Chung, C.F., Fabbri, A.G., 2001. Prediction models for landslide hazard using fuzzy set approach. In: Marchetti, M., Rivas, V. (Eds.), Geomorphology and Environmental Impact Assessment. A.A. Balkema, Rotterdam, pp. 31–47.

Chung, C.F., Fabbri, A.G., Van Westen, C.J., 1995. Multivariate regression analysis for landslide hazard zonation. In: Carrara, A., Guzzetti, F. (Eds.), Geographical Information Systems in Assessing Natural Hazards. Kluwer Academic Publishers, Dordrecht, The Netherlands, pp. 107–133.

Connell, L.D., Jayatilaka, C.J., Nathan, R., 2001. Modelling flow and transport in irrigation catchments, spatial application of subcatchment model. Water Resources Research 37 (4), 965–977.

Dietrich, E.W., Reisss, R., Hsu, M.L., Montgomery, D.R., 1995. A process-based model for colluvial soil depth and shallow landsliding using digital elevation data. Hydrological Processes 9, 383–400.

Du, R.H., Kang, Z.C., Chen, X.Q., 1987. Comprehensive investigation, prevention and planning of debris flow in Xiaojiang watershed, Yunnan Science and Technology Press, Chongqing, China (in Chinese).

Guzzetti, F., Carrara, A., Cardinali, M., Reichenbach, P., 1999. Landslide evaluation: a review of current techniques and their application in a multi-scale study, Central Italy. Geomorphology 31, 181–216.

Grayson, R.B., Moore, I.D., McMahon, T.A., 1992. Physically based hydrologic modeling: 1. A terrain-based model for investigative purposes. Water Resources Research 28 (10), 2639–2658.

Heckerman, D., 1986. Probabilistic interpretation of MYCIN's certainty factors. In: Kanal, L.N., Lemmer, J.F. (Eds.), Uncertainty in Artificial Intelligence. Elsevier, New York, pp. 298–311.

Jade, S., Sarkar, S., 1993. Statistical models for slope stability classification. Engineering Geology 36, 91–98.

Kim, W., Garza, J., Keskin, A., 1993. Spatial data management in database systems: research directions. Advances in Spatial Database. Springer, Berlin.

Luzi, L., Pergalani, F., 1999. Slope instability in static and dynamic conditions for urban planning: the 'Oltre Po Pavese' case history (Regione Lombardia-Italy). Natural Hazards 20, 57–82.

Montgomery, D.R., Dietrich, W.E., 1994. A physically based model for the topographic control on shallow landsliding. Water Resources Research 30 (4), 1153–1171.

Pack, R.T., Tarboton, D.G., Goodwin, C.N., 1998. The SINMAP approach to terrain stability mapping. Proceedings of 8th Congress of the International Association of Engineering Geology, Vancouver, British Columbia, Canada, pp. 1157–1165.

Shortliffe, E.H., Buchanan, G.G., 1975. A model of inexact reasoning in medicine. Mathematical Biosciences 23, 351–379.

Van Westen, C.J., 1994. GIS in landslide hazard zonation: a review with examples from the Colombian Andes. In: Price, M.F., Heywood, D.I. (Eds.), Taylor and Francis, London, pp. 35–65.

Wu, W., Sidle, R.C., 1995. A distributed slope stability model for steep forested watersheds. Water Resources Research 31 (8), 2097–2110.

Wu, J.S., Kang, Z.C., Tian, L.Q., Zhang, S.C., 1990. Monitoring on Debris Flow in Jiangjiagou Watershed, Yunnan Science Press, Beijing, China (in Chinese).